4 Pipe Failure Modes and Failure Criterion

This chapter describes the failure modes for buried pipelines subject to seismic loading. The principal failure modes for corrosion-free continuous pipelines (e g. steel pipe with welded joints) are rupture due to axial tension, local buckling due to axial compression and flexural failure. If the burial depth is shallow, continuous pipelines in compression can also exhibit beam-buckling behavior. Failure modes for corrosion-free segmented pipelines with bell and spigot type joints are axial pull-out at joints, crushing at the joints and round flexural cracks in pipe segments away from the joints. For each of these failure modes, the corresponding failure criterion is presented, first for continuous pipelines and then for segmented pipelines.

4.1 Continuous Pipeline

The principal failure modes for corrosion-free continuous pipeline with burial depth of about three feet or more are tensile rupture and local buckling. Buried pipelines with burial depths less than about 3 feet (i.e , shallow trench installation) may experience beam buckling behavior. Beam buckling has also occurred during post earthquake excavation undertaken to relieve compressive pipe strain.

4.1.1 Tensile Failure

When strained in tension, corrosion free steel pipe with arc welded butt joints is very ductile and capable of mobilizing large strains associated with significant tensile yielding before rupture.

On the other hand, older steel pipe with gas-welded joints often cannot accommodate large tensile strain before rupture. In addition, as discussed in detail in Section 4.1.4, welded slip joints in steel pipe do not perform as well as butt welded joints. The 1994 Northridge event provides a case history of these differences in behavior. According to T. O'Rourke and M. O'Rourke (1995), none of the four arc-welded steel pipes with butt joints along Balboa Blvd suffered tensile rupture when subjected to longitudinal PGD. However three gas-welded pipes with slip joints suffered tensile rupture when subjected to the same PGD.

The strain associated with tensile rupture is generally well above about 4% (Newmark and Hall, 1975). Often an ultimate tensile value of 4% is used, beyond which the pipeline is considered to have failed in tension.

Analytical methods for post-yield performance require full descriptions of the stress-strain behavior. One of the most widely used models is the one proposed by Ramberg and Osgood (1943). The Ramberg Osgood model is given by:

$$\varepsilon = \frac{\sigma}{E}\left[1 + \frac{n}{1+r}\left(\frac{\sigma}{\sigma_y}\right)^r\right] \tag{4.1}$$

where ε is the engineering strain, σ is the uniaxial tensile stress, E is the initial Young's modulus, σ_y is the apparent yield stress, n and r are Ramberg Osgood parameters. Commonly used values for σ_y, n and r for various grades of steel are listed in Table 4.1. The Ramberg Osgood relationship will be used in determining the response of continuous pipe subject to longitudinal PGD in Chapter 6.

■ Table 4.1 Ramberg Osgood Parameters for Mild Steel and X-grade Steel

	Grade-B	X-42	X-52	X-60	X-70
Yield Stress (MPa)	227	310	358	413	517
n	10	15	9	10	5.5
r	100	32	10	12	16.6

4.1.2 Local Buckling

Buckling refers to a state of structural instability in which an element loaded in compression experiences a sudden change from a stable to an unstable condition. Local buckling (wrinkling) involves local instability of the pipe wall. After the initiation of local shell wrinkling, all further geometric distortion caused by ground deformation or wave propagation tends to concentrate at the wrinkle. The resulting large curvatures in the pipe wall often then lead to circumferential cracking of the pipe wall and leakage. This is a common failure mode for steel pipe. Wave propagation in the 1985 Michoacan event caused this type of damage to a water pipe in Mexico City. Permanent ground deformation caused this type of damage to a liquid fuel pipeline in the 1991 Costa Rica event, as shown in Figure 4.1, and to water and gas pipelines in the 1994 Northridge event.

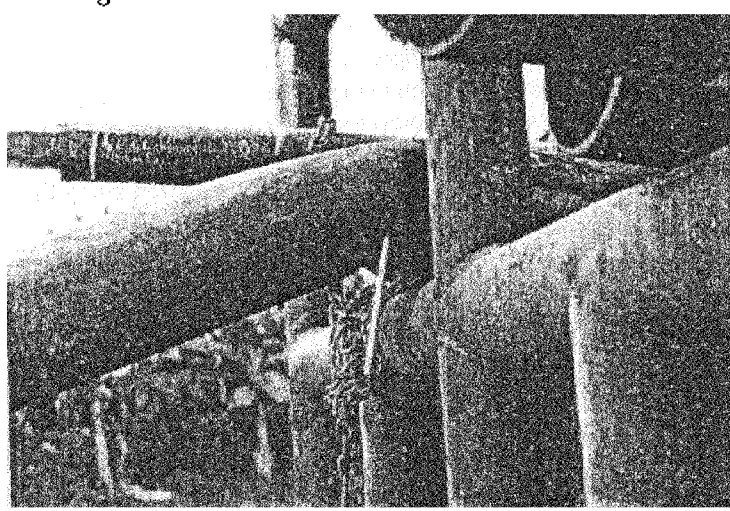

After M. O'Rourke and Ballantyne, 1992

■ Figure 4.1 Local Buckling to RECOPE Pipeline

Based on prior laboratory tests on thin wall cylinders, Hall and Newmark (1977) suggest that compressional wrinkling in a pipe normally begins at a strain of 1/3 to 1/4 of the theoretical value of:

$$\varepsilon_{theory} = 0.6 \cdot t/R \qquad (4.2)$$

where t is the pipe wall thickness and R is the pipe radius. Hence, in terms of failure criterion the onset of wrinkling occurs at strains in the range.

$$0.15 \cdot t / R \leq \epsilon_{cr} \leq 0.20 \quad t / R \tag{4.3}$$

This assumed wrinkling strain is thought to be appropriate for thin wall pipe but somewhat conservative for thicker wall pipe. The additional amount of longitudinal compressive deformation across the wrinkled zone which results in tearing of the pipe wall due to large curvature at individual wrinkles is, at present, not well established

4.1.3 Beam Buckling

Beam buckling of a pipeline is similar to Euler buckling of a slender column in which the pipe/column undergoes a transverse upward displacement. The relative movement is distributed over a large distance and hence the compressive pipe strains are not large. As a result beam buckling of a pipeline in a ground compression zone is considered more desirable than local buckling since the potential for tearing of the pipe wall is lessened.

Beam buckling of pipes has been observed in a few events. For example, during the period from 1932 to 1959, displacements on the order of 360 mm (14 in.) accumulated across the Buena Vista reverse fault (Howard, 1968). This ground movement led to compression stresses in oil pipelines, ranging from 51 to 406 mm (2 to 16 in.) in diameter. The oil pipelines buried at depths between 0.15 and 0.30 m (6 to 12 in.), and in loose to medium soil, lifted out of the ground as a result of compressive forces.

Another example occurred during the 1979 Imperial Valley earthquake. Two high pressure pipelines, 219 mm (8.6 in.) and 273 mm (10.7 in.) in diameter, crossing the main trace of the Imperial fault were affected. No evidence of local buckling or beam buckling was observed immediately after the event. However, removal of cover during inspection after the earthquake caused both pipes to displace laterally in a beam buckling mode (McNorgan, 1989).

As opposed to tensile rupture, or wrinkling and associated tearing of the pipe wall, the pipes do not "fail" after beam buckling. The beam bucking of pipes may better be described as a serviceability problem since the pipe continues to serve its function of transmitting fluid without interruption. In that sense it is difficult to establish a failure criterion for beam buckling strictly in terms of pipe material properties. Its occurrence depends on several factors such as the bending stiffness and burial depth of the pipe as well as initial imperfections. A discussion of the conditions leading to beam buckling is presented below.

Beam buckling of buried pipelines has been the subject of many analytical studies. An analytical solution for a type of beam buckling was first provided by Marek and Daniels (1971). They studied the behavior of continuous crane rails subject to a temperature rise. Hobbs (1981) adapted the Marek and Daniels model to solve the problem of buckling of submarine pipelines. Hobbs considered the compressive loads due to temperature changes or internal pressures, which can cause beam buckling in the presence of an initial imperfection. His model is shown in Figure 4.2, where w is the submerged weight of pipeline per unit length, L_b is the length of the buckle, L_s is the length of pipe adjacent to the buckle which slips with respect to the surrounding soil.

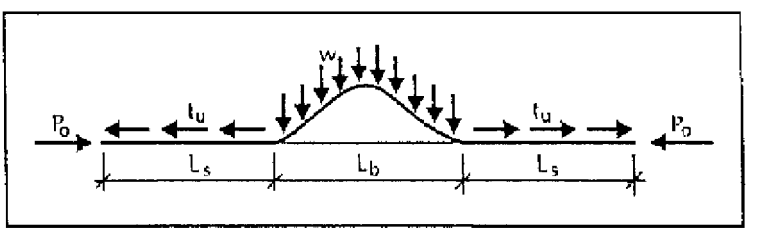

After Hobbs 1981

■ **Figure 4.2 Vertical Buckling Mode**

Figure 4.3 shows the buckling load versus the buckling length, L_b, and the maximum buckling amplitude, y_o.

As shown in Figure 4.3, the buckling load is a nonlinear function of buckling length and achieves a minimum value at Point B for a certain buckling length, $L_{b_{min}}$. Due to uplift resistance and soil

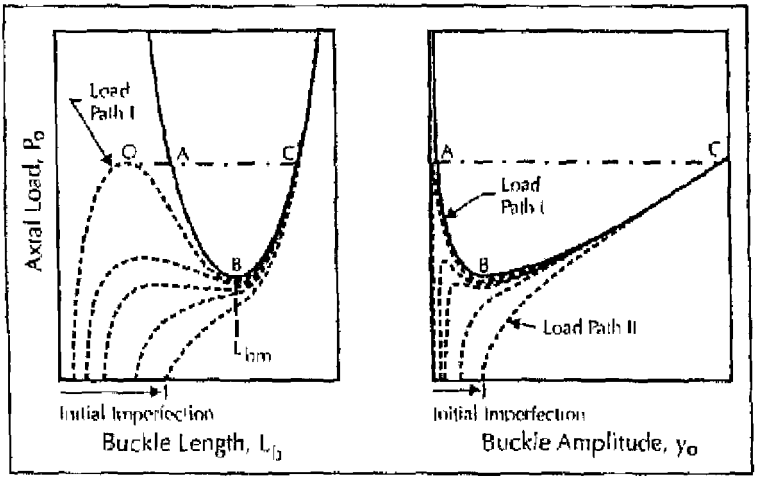

After Hobbs, 1981

■ Figure 4.3 Vertical Buckling Load and Equilibrium Paths for Increasing Imperfection Level

friction, the buckling load increases for the buckling length larger than L_{imp}. Obviously, for any load higher than that at Point B, there are two possible buckling lengths and amplitudes, for example, values at Point A and Point C in Figure 4.3. The situation at Point A is unstable and the pipe will tend to eventually snap through to Point C at a constant axial load. Note that, for the case of small initial imperfection, the pipe buckles and the post-buckling curve is shown, for example, in Path I after the compressive load reaches the maximum value at Point O. On the contrary, for large initial imperfection case, no snap-through is observed (for example, Path II) since the imperfection is gradually magnified in this case.

Kyriakides et al. (1983) used a somewhat similar approach more recently which requires imperfection information. Ariman and Lee (1989) augmented the Kyriakides et al.'s model by considering an axial friction force at the pipe-soil interface, nonlinear uplift resistance, as well as an elasto-plastic moment-curvature relation for the pipe. One difficulty in applying both the Kyriakides et al. or the Ariman and Lee model in practice, is that information on typical pipeline imperfections is apparently not readily available.

Meyersohn (1991) overcame this difficulty by extending Hobbs procedure to the problem of beam buckling of buried pipelines subject to longitudinal PGD. Figure 4.4 shows the distribution of

axial compressive forces before buckling and after buckling. The length of the stressed portion of the pipe is directly associated with the magnitude and extent of the ground displacement. Once the axial force in the pipe P equals or exceeds a certain value, referred to as P_{max}, beam buckling occurs. The frictional forces are then relieved over the uplifted length of the pipe. The frictional forces also change direction over portions of the pipe at both sides of the buckle (i.e., the zone of reversed friction in Figure 4.4(b)), relieving some axial stress. The force P_o represents the maximum axial force after equilibrium is restored.

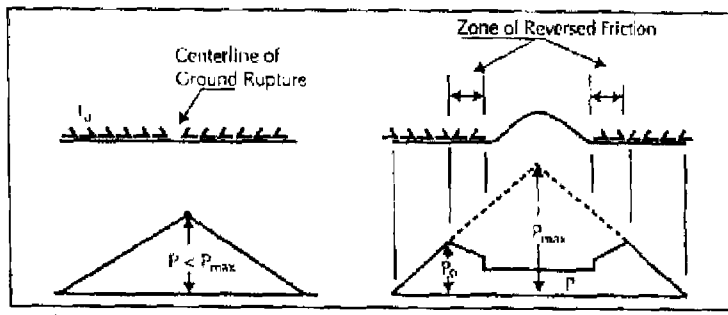

After Meyersohn, 1991

■ **Figure 4.4 Distribution of Axial Compressive Forces**

Intuitively, beam buckling is more likely to occur in pipelines buried in shallow trenches and/or backfilled with loose materials. That is, beam buckling load is an increasing function of the cover depth. Hence, if a pipe is buried at a sufficient depth, it will develop local buckling before beam buckling. Based on this concept, Meyersohn (1991) determined a critical cover depth by setting the lowest beam buckling stress equal to local buckling stress. Any pipe buried with less cover than the critical depth would experience beam buckling before local buckling. Conversely, if the pipe is buried at a depth more than the critical depth, it will experience local buckling. Figure 4.5 shows the critical cover depth for Grade B and X-60 steel pipes.

The shaded areas in the figure correspond to different degrees of backfill compaction. Note that critical depth for X-60 steel is larger than that for Grade B steel. That is, the stronger the pipe, the

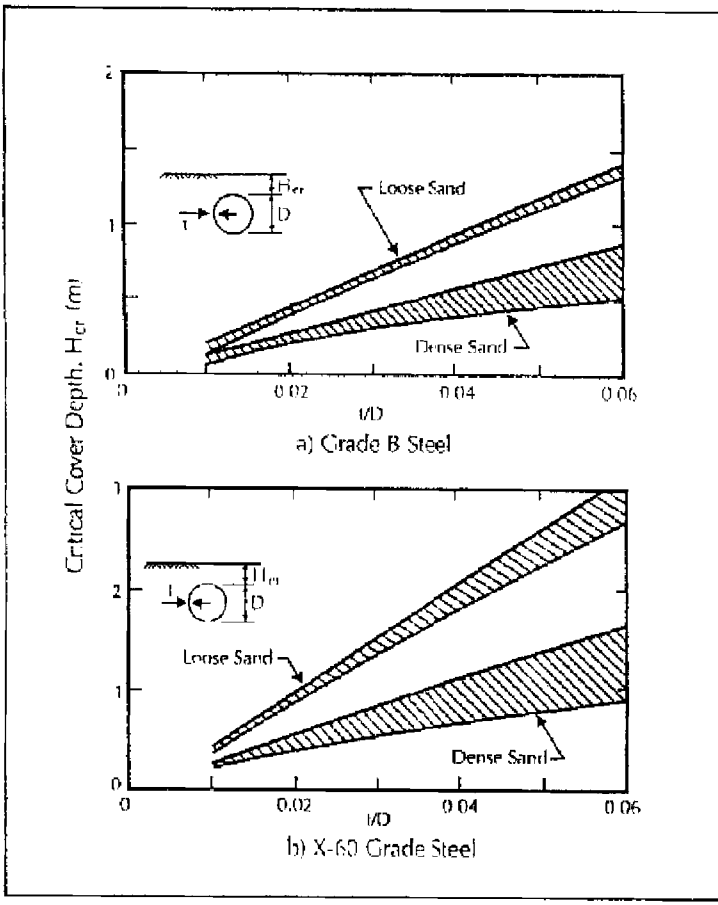

After Meyersohn 1991

■ Figure 4.5 Analytical Critical Cover Depth of Pipe for Grade B and X-60 Steel

smaller the possibility of shell wrinkling as opposed to beam buckling. However, as noted by Meyersohn (1991), the *H/D* ratio is typically less than or about equal to 0.02. Hence, from Figure 4.5, the likelihood of beam buckling of buried pipelines is small since the critical depth is less than typical burial depths.

4.1.4 WELDED SLIP JOINTS

The failure criterion for steel pipelines with arc-welded butt joints is based on the strength of pipe material as discussed previously. However, for steel pipelines with slip joints, riveted joints or oxy-acetylene/gas welded joints, failure criterion is based on the strength of these joints since it is less than that of pipe materials. Many such steel pipelines have suffered failure at those joints during past earthquakes. For example, during the 1971 San Fernando earthquake, the Granada Trunk line (1260 mm in diameter) was damaged at its welded slip joints (T. O'Rourke and Tawfik, 1983). Figure 4.6 shows a slip joint where t is the pipe wall thickness.

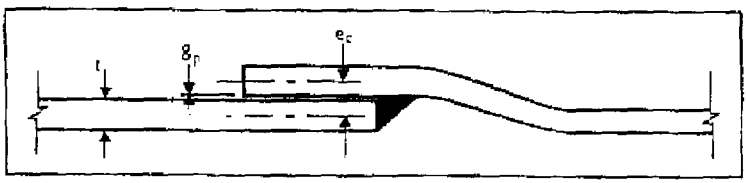

After Brockenbrough, 1990

■ Figure 4.6 Slip Joint with Inner Weld

Tawfik and T. O'Rourke (1985), Moncarz et al. (1987), and Brockenbrough (1990) analyzed the strength of slip joints. Considering 108 inch (2.74 m) diameter pipe with an inner weld, Moncarz et al. calculated a joint efficiency of 0.4 (strength of joint compared to strength of pipe) by using an inelastic finite element model. Considering the same type of joints, Brockenbrough determined a joint efficiency of 0.35, which is a little less (12%) than Moncarz et al.'s result. Figure 4.7 presents the joint efficiency of bell-spigot joints with an inner weld by Brockenbrough's model. Note that the maximum efficiency is 0.41, when no space or gap exists between the bell and spigot walls, and the joint efficiency is a decreasing function of the gap.

However, for most pipelines, slip joints with an outer weld are used since it is difficult to weld inside portions of pipe segments when the pipe diameter is small. Figure 4.8 shows a slip joint with an outer weld.

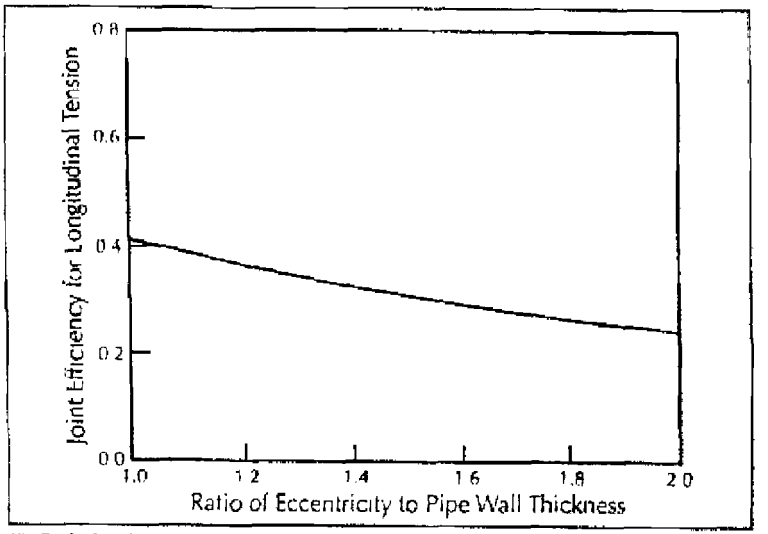

After Brockenbrough 1990

■ Figure 4.7 Joint Efficiency for Slip Joints with Inner Weld

As shown in Figure 4.6(b), t is the wall thickness, R_o is the pipe radius, e is the eccentricity (offset of the joint) and l is the length of curved portion of bell. Using an inelastic shell model, Tawfik and T. O'Rourke (1985) calculate joint efficiencies as shown in Figure 4.9. Note that two failure modes are considered in their analyses. Mode I refers to yielding in the vicinity of welded connections and Mode II refers to plastic flow in the curvilinear, belled

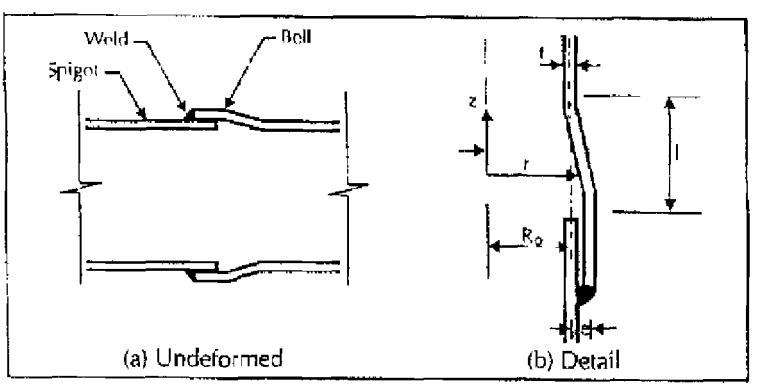

After Tawfik and T. O'Rourke, 1985

■ Figure 4.8 Slip Joint with Outer Weld

ends of the joints. For normalized length of the bell $l/R_0 > 0.30$, Mode I governs and the joint efficiency is about 0.29.

As shown in Figure 4.7 and Figure 4.9, the joint efficiency of slip joints with an inner weld is often larger than that with an outer weld. Presumably this is because the eccentricity of the weld with respect to the pipe radius for joints with an inner weld are smaller than that with an outer weld.

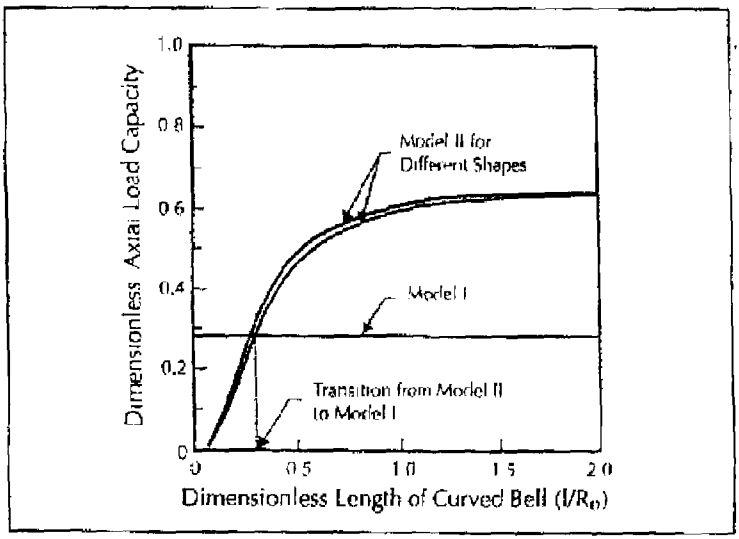

After Tawfik and T. O'Rourke, 1985

■ Figure 4.9 Joint Efficiency of Slip Joints with an Outer Weld

4.2 SEGMENTED PIPELINE

For segmented pipelines, particularly those with large diameters and relatively thick walls, observed seismic failure is most often due to distress at the pipe joints. For example, in the 1976 Tangshan earthquake, Sun and Shien (1983) observed that around 80 percent of pipe breaks were associated with joints. M. O'Rourke and Ballantyne (1992) identified six types of damage mechanism

to segmented pipelines shown in Figure 4.10 during the 1991 Costa Rica earthquake. For the CI and DI transmission pipelines in the Limon area, 52% repairs are due to pull-out at joints (Figure 4.10(f)) and 42% repairs are due to breaks at segments (Figure 4.10(a))

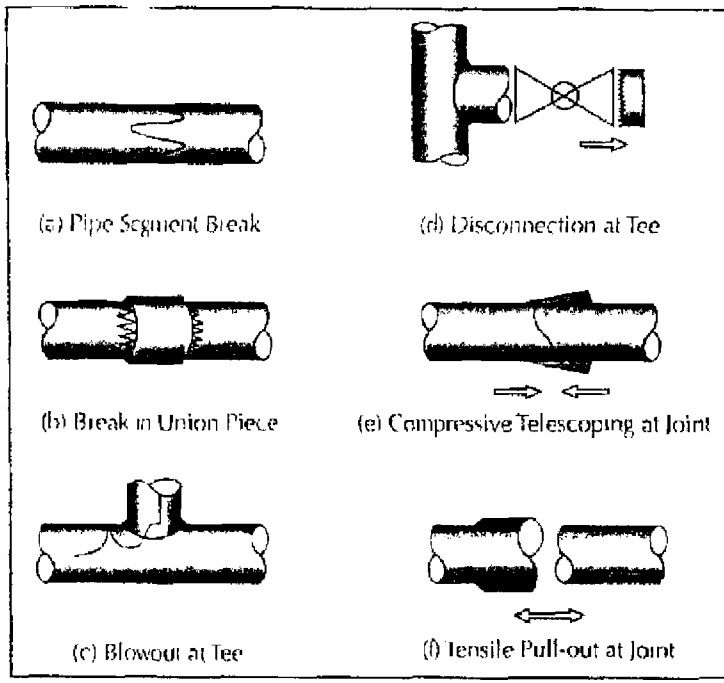

After M. O'Rourke and Ballantyne, 1992

■ Figure 4.10 Damage Mechanisms for Segmented Pipelines

Axial pull-out, sometimes in combination with relative angular rotation at joints, is a common failure mechanism in areas of tensile ground strain since the shear strength of joint caulking materials is much less than the tensile strength of the pipe. In areas of compressive ground strain, crushing of bell and spigot joints is a fairly common failure mechanism in, for example, concrete pipes. For small diameter segmented pipes, circumferential flexural failure have been observed in areas of ground curvature. For example, as observed by T. O'Rourke et al. (1991), more than 80 percent of

the breaks in cast iron pipes with small diameters (100 mm to 200 mm (4 to 8 in)) in the Marina district after the 1989 Loma Prieta event were round cracks in pipe segments close to joints.

4.2.1 AXIAL PULL-OUT

In terms of failure criterion, information for the various types of segmented pipes is not as well developed as for continuous pipes. El Hmadi and M. O'Rourke (1989) summarized the then available information on joint pull-out failure. Specifically, based on laboratory tests by Prior (1935), El Hmadi and M. O'Rourke (1989) established a cumulative distribution for leakage as a function of the normalized joint axial displacement u_l''/d_p shown in Figure 4.11. Note that u_l'' is the joint opening and d_p is the joint depth.

As shown in Figure 4.11, the mean value of the joint opening corresponding to joint leakage is 0.52 d_p with a coefficient of variation of 10%. Hence, El Hmadi and M. O'Rourke suggest a relative joint displacement corresponding to 50% of the total joint depth as the failure criterion for pull-out of segmented pipelines with "rigid" joints.

For ductile iron pipes with rubber gasketed joints, they present laboratory data and semi-empirical relations developed by Singhal (1983) for the ultimate axial tensile force in the joint at pull-out

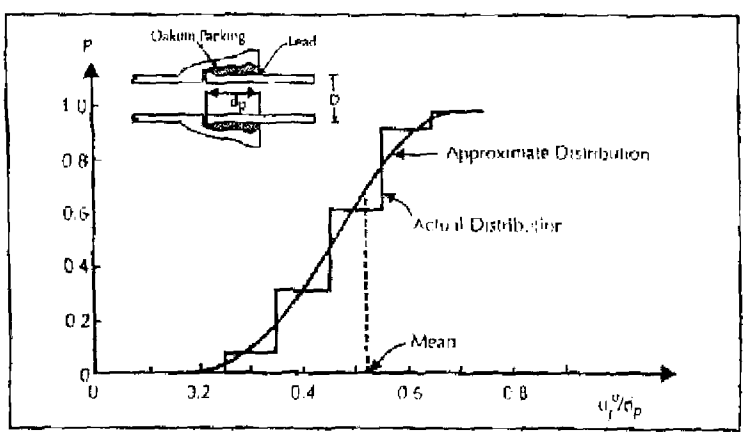

El Hmadi and M. O'Rourke, 1989

Figure 4.11 Cumulative Distribution Function for Leakage of Lead Caulked Joints

More recently, laboratory tests on concrete cylinder pipes with rubber gasketed joints by Bouabid and M. O'Rourke (1994) suggest that, at moderate internal pressures, the relative joint displacement leading to significant leakage corresponds to roughly half the total joint depth. Hence, it would appear that a relative axial joint extension of roughly half the total joint depth may be an appropriate failure criterion for many types of segmented pipes.

4.2.2 Crushing of Bell and Spigot Joints

As noted by Ayala and M. O'Rourke (1989), most of the concrete cylinder pipe failures in Mexico City occasioned by the 1985 Michoacan event were due to joint crushing. The corresponding failure criterion, based on laboratory tests for crushing of bell and spigot joints, is apparently not well established at this time.

According to Bouabid and M. O'Rourke's observation in their 1993 axial compressive tests, joint failure to reinforced concrete cylinder pipes with rubber gasketed joints can start at either the inner concrete lining or the outer concrete lining. That is, a circumferential crack starts to form in the ends of the concrete lining when the applied load nears the ultimate value. After concrete lining cracks, the critical section then becomes the welded interface between the steel joint ring and the steel pipe cylinder. The eccentricity existing between these two-elements causes some denting (or even local buckling) near this welded region. Such damaging action eventually would result in a leakage path and/or cause the section to burst. Hence, both Bouabid and M. O'Rourke (1994) as well as Krathy and Salvadori (1978) proposed that the crushing failure criterion for concrete pipes can be taken as the ultimate compression force of the concrete core at joints, F_{cr}. That is,

$$F_{cr} = \sigma_{ccomp} \cdot A_{core} \tag{4.4}$$

where σ_{ccomp} is the compressive strength of concrete and A_{core} is the area of the concrete core. For plain concrete pipes, A_{core} is the cross-section area, while for reinforced pipes, the transformed area of steel bars needs to be added.

4.2.3 Circumferential Flexural Failure and Joint Rotation

When a segmented pipeline is subject to bending induced by lateral permanent ground movement or seismic shaking, the ground curvature is accommodated by some combination of rotation at the joints and flexure in the pipe segments. The relative contribution of these mechanisms depends on the joint rotation and pipe segment flexural stiffnesses. For a flexible pipeline system such as DI pipe with Tyton joints or FLEX joints, stress in the pipe segments starts to increase greatly only after the joint rotation capacity, typically about 4° and 15° respectively, is exceeded. On the other hand, for a more rigid segmented pipeline system such as cast iron pipe with cement/lead joints, ground curvature is accommodated from the start by some combination of joint rotation and flexure in the segments as will be discussed in more detail in Chapter 11.

In terms of failure criterion, it seems reasonable to base joint rotation failure/leakage criterion for "standard" segmented pipeline joints on some multiple (say 1.1 to 1.5) of the allowable angular offset for pipe laying purposes contained in manufacturer's literature. Table 4.2 contains a listing of such manufacturer's recommended allowable offset.

For cast iron or asbestos cement pipes subject to ground curvature, round flexural cracks in segments are a major failure mode. On the other hand, for concrete pipes subject to ground curvature, cracks typically occur at the bell and spigot ends due in part to the joint ring eccentricity mentioned previously.

For round flexural cracks, it seems reasonable to use, as a failure criterion, the pipe curvature corresponding to the smaller of the ultimate tensile or compressive strains for the material. In this regard El Hmadi and M. O'Rourke (1989) presented a listing of these mechanical properties for CI and DI pipe materials. Table 4.3 summarizes this information as well as the properties for other common pipe materials

■ Table 4.2 Typical Manufacturer's Recommended Allowable Angular Offset (deg. and min.) for Various Pipe Joints

D (in)	Cast Iron	Ductile Iron		Prestressed Concrete	Concrete
		Push-on	Mechanical		
4	4-00	5	8-18		
6	3-30	5	7-07		
8	3-14	4	5-21		
10		4	5-21		
12	3-00	4	5-21		
14		3	3-35		
16	2-47	3	3-35		2-19
18		3	3-00		2-04
20	2-09	3	3-00		1-52
24	1-47	2	2-23		1-34
27		2	2-23		1-24
30	1-26	2	2-23	1-44	1-15
36		1-30		1-35	1-09
36		1-30	2-05	1-28	1-03
42		1-30	2-00	1-16	1-03
48		1-30	2-00	1-06	1-03
60		1-30		0-56	
72		1-30		0-56	

■ Table 4.3 Mechanical Properties for Common Pipe Materials

Item	Cast Iron	Ductile Iron	Concrete	PVC	HDPE
Yield Strain $\times 10^{-3}$	1.0 to 3.0	1.75 to 2.17	0.1 to 1.3	17 to 22	22 to 25
Ultimate Strain $\times 10^{-3}$	5.0 to 40	100	0.25 to 3.0	50 to >100	50 to >100
Yield Stress (ksi)	14 to 42	42 to 52	0.32 to 4.0	5.0 to 6.5	2.2 to 2.5
Initial Modulus (ksi)	14,000	24,000	3,000	290-560	100-120